Revealing an unusual transparent phase of superhard iron tetraboride under high pressure

Komsilp Kotmool[a], Thanayut Kaewmaraya[b], Sudip Chakraborty[b], Jonas Anversa[c], Thiti Bovornratanaraks[a,d], Wei Luo[b], Huiyang Gou[e], Paulo Cesar Piquini[c], Tae Won Kang[f], Ho-kwang Mao[e,g,1], and Rajeev Ahuja[b,f,h,1]

[a]Center of Excellence in Forum for Theoretical Science, Department of Physics, Faculty of Science, Chulalongkorn University, Bangkok 10330, Thailand; [b]Condensed Matter Theory Group, Department of Physics and Astronomy, Uppsala University, S-75120 Uppsala, Sweden; [c]Departamento de Física, Universidade Federal de Santa Maria, 97105-900 Santa Maria, Rio Grande do Sul, Brazil; [d]Thailand Center of Excellence in Physics, Commission on Higher Education, Bangkok 10400, Thailand; [e]Geophysical Laboratory, Carnegie Institution for Science, Washington, DC 20015; [f]Quantum Functional Semiconductor Research Center, Dongguk University, Chung gu, Seoul 100-715, Korea; [g]Center for High Pressure Science and Technology Advanced Research, Shanghai 201203, People's Republic of China; and [h]Applied Materials Physics, Department of Materials and Engineering, Royal Institute of Technology, S-100 44 Stockholm, Sweden

Contributed by Ho-kwang Mao, October 8, 2014 (sent for review August 30, 2014)

First principles–based electronic structure calculations of superhard iron tetraboride (FeB_4) under high pressure have been undertaken in this study. Starting with a "conventional" superconducting phase of this material under high pressure leads to an unexpected phase transition toward a semiconducting one. This transition occurred at 53.7 GPa, and this pressure acts as a demarcation between two distinct crystal symmetries, metallic orthorhombic and semiconducting tetragonal phases, with *Pnnm* and $I4_1/acd$ space groups, respectively. In this work, the electron–phonon coupling-derived superconducting T_c has been determined up to 60 GPa and along with optical band gap variation with increasing pressure up to 300 GPa. The dynamic stability has been confirmed by phonon dispersion calculations throughout this study.

metal–semiconductor phase transition | superhard material | first principle study | high pressure | superconductivity

The shorter interatomic distances of metal under external pressure consequently increase the valence and conduction band widths, which leads to the enhancement of free electron-like behavior. The development of creating immensely substantial pressure at laboratories enables us to observe the core electrons overlapping under enormous compression and dramatically influences the electronic properties of normally free electron metals such as Li and Na (1–3). The metal-to-insulating phase transformation has been contrived both experimentally and theoretically for both the normal metals while exerting pressure on them. This observation propelled us to investigate the electronic and structural phase transformation of the experimentally synthesized superhard material iron tetraboride (FeB_4) under high pressure (4–8). The intriguing factor of choosing FeB_4 is that the material was proposed as a "conventional" Fe-based superconductor, in contradiction to the discovery of an "unconventional" Fe-based superconductor because of its large electron–phonon coupling. Here we report the exotic phase transition of FeB_4 from metal to semiconductor at 53.7 GPa, even though we started with the metallic orthorhombic phase *Pnnm* of FeB_4, which shows the superconducting temperature T_c up to 60 GPa. The new phase after 53.7 GPa has $I4_1/acd$ space group symmetry with a finite fundamental band gap, which increases along with pressure monotonically. All of the considered structures have been tested to have a thermodynamic stability from phonon dispersion calculations. The reason behind the phenomena could be the overlap of atomic cores at higher pressure ranges, which increases the hybridization of valence electrons and their repulsive interactions with core electrons. The immediate technological outcome of this scenario of metal-to-semiconducting phase transition could be to search for a transparent state of a material that is a metal under ambient conditions. This drastic change of electronic and structural properties can be observed in other materials as well, and hence this can open a field of studying them from a high-pressure perspective.

Results and Discussion

We have started compressing the *Pnnm* structure, which has equilibrium lattice constants $a_0 = 4.52$ Å, $b_0 = 5.27$ Å, and $c_0 = 3.00$ Å. Using the Birch–Murnaghan equation of state, the equilibrium cell volume (V_0), bulk modulus (B_0), and the first derivative (B_0') are fitted to be 35.80 $Å^3$ per formula unit (f.u.), 270.1 GPa, and 3.64, respectively, reproducing well the experimental values (V_0 = 36.38 $Å^3$/f.u., B_0 = 252.5 GPa, and $B_0' = 3.53$) (5). While compressing the initial structure (Fig. 1), we have found that after 53.7 GPa another possible structure has emerged that is more energetically favorable as far as the enthalpy contribution is concerned. The new structure that has been predicted by the evolutionary algorithm (USPEX) (9, 10) has the symmetry $I4_1/acd$ tetragonal phase. The first-order phase transition occurred while transforming from *Pnnm* to $I4_1/acd$ with the relative volume contraction of 4%. The $I4_1/acd$ phase has B_0 = 311.5 GPa and $B_0' = 3.87$ with the lattice constants a = 4.84 Å, c = 9.73 Å, and the atomic positions of Fe (16c) at (0.500, 0.000, 0.000) and of B (32g) at (0.125, 0.130, 0.062) at 53.7 GPa. The other possible structure with the second-lowest enthalpy is the $P4_2/nmc$ phase, which possesses B_0 = 307.0 GPa and $B_0' = 3.95$ with the lattice constants a = 3.46 Å, c = 4.87 Å with the atomic positions of Fe(2a) at (0.00, 0.00, 0.00)

Significance

Solids have been mainly studied at ambient conditions (i.e., at room temperature and zero pressure). However, it was realized early that there is also a fundamental relation between volume and structure and that this dependence could be most fruitfully studied by means of high-pressure experimental techniques. From a theoretical point of view this is an ideal type of experiment, because only the volume is changed, which is a very clean variation of the external conditions. In the present study we show a hard superconducting material, iron tetraboride, transforms into a novel transparent phase under pressure. Further, this phase is the first system in this class, to our knowledge, and opens a new route to search for and design new transparent materials.

Author contributions: R.A. designed research; K.K., T.K., S.C., and J.A. performed research; K.K., T.K., S.C., T.B., W.L., H.G., P.C.P., T.W.K., H.-k.M., and R.A. analyzed data; and K.K., T.K., S.C., and R.A. wrote the paper.

The authors declare no conflict of interest.

[1]To whom correspondence may be addressed. Email: mao@gl.ciw.edu or rajeev.ahuja@physics.uu.se.

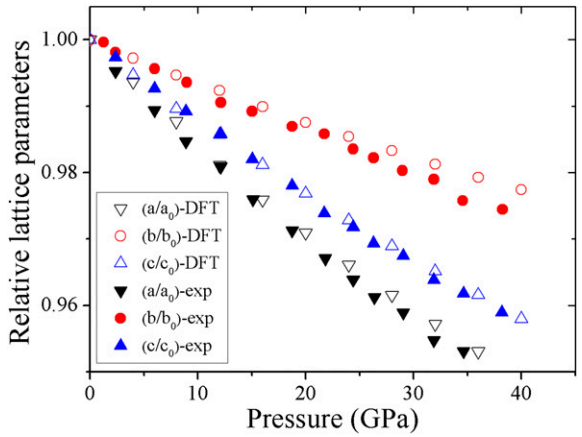

Fig. 1. The comparison of normalized lattice parameters of FeB_4 (*Pnnm* phase) between the present work (open symbols) and the experimental findings (closed symbols).

and of B (8g) at (0.25, 0.00, 0.369) at 58 GPa. The enhanced bulk modulus of $I4_1/acd$ and $P4_2/nmc$ phases indicate that they are harder than the ambient structure. Although a previous study reported the dynamic stability of the (*Pnnm*) phase from 0 to 100 GPa (6), the phonon dispersion of the $I4_1/acd$ phase at 53.7 GPa as shown in Fig. 2 reveals the dynamic stability and it is even maintained up to 300 GPa. The top and side views of the considered atomic structures are depicted in Fig. 3.

It is worth mentioning that the tetragonal with space group $P4_2/nmc$ emerges in parallel with the formation enthalpy higher (around 30 meV/f.u.) than $I4_1/acd$, as indicated in Fig. 4, and the structure also shows dynamic stability at 53.7 GPa up to 300 GPa. This suggests that these two tetragonal phases may be mutually found in experiments within the same pressure range. In addition, the structures having space group $C2/m$, $R3m$, and $P6_3mc$ are the other possible candidate structures, which have been derived from the USPEX, but their enthalpies are relatively higher than the $I4_1/acd$ phase with a minimum value of 300 meV/f.u.

Fig. 5*A* depicts the pressure dependence of electron–phonon coupling constant (λ), the superconducting critical temperature (T_c), and logarithm of phonon momentum (ω_{log}) for the *Pnnm* structure. At ambient pressure, the T_c is calculated to be 2.72 K by using the effective Coulomb repulsion parameter (μ^*) of 0.18. We have additionally performed the tests using different values of μ^* such as 0.10 and 0.14 and we have found the corresponding T_c values to be 9.35 K and 5.50 K, respectively. Hence, the T_c

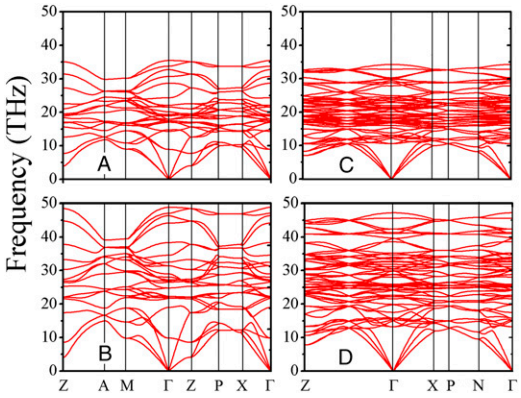

Fig. 2. Phonon dispersions of $I4_1/acd$ (*A* and *B*) and $P4_2/nmc$ (*C* and *D*) at pressure 53.7 and 300 GPa, respectively.

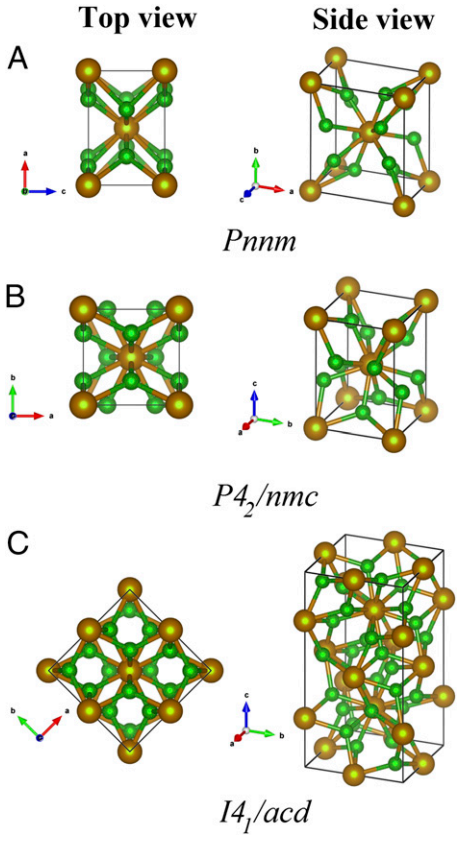

Fig. 3. Top and side view of atomic structures of (*A*) *Pnnm*, (*B*) $P4_2/nmc$, and (*C*) $I4_1/acd$. Fe and B atoms are shown as brown and green balls, respectively.

evaluated by the stronger μ^* of 0.18 quantitatively agrees with the experimental value of 2.9 K (5), because Fe-*d* electrons are strongly localized near the Fermi level (11). Under compression, the λ monotonically gets suppressed, resulting in a drop of T_c at increasing pressure. However, the anomalous recovery of λ and T_c is found at 60 GPa, which is associated with the softening of phonons to yield the strong electron–phonon coupling. Further, the calculated spectral function $\alpha^2F(\omega)$ and integrated $\lambda(\omega)$ at the selected pressure points shown in Fig. 6 reveal that the low-frequency regime (0 to around 350 cm^{-1}), which originates from Fe-B vibration, significantly contributes to λ. Therefore, we conclude that the observed superconductivity of the *Pnnm* phase is mainly attributed to the strong coupling of Fe-B vibration at low frequencies.

We have established the pressure-induced phase transition from *Pnnm* to $I4_1/acd$, and the details regarding their electronic structures are presented in Fig. 7. The *Pnnm* phase exhibits a nonsemiconducting behavior both at 0 and 60 GPa, which is typically characterized by finite states at the Fermi level owing to the hybridization between Fe-3*d* states and B-2*p* states. We find the bands crossing the Fermi level at $\Gamma \rightarrow Z$ and $U \rightarrow R$, which corresponds to the 3D Fermi surface centered at Γ and *R* points (4). These flat bands coming from Fe-*d* and B-*p* states are crucial for the observed superconductivity in FeB_4 as previously described. By contrast, the $I4_1/acd$ at 53.7 GPa does exhibit a semiconducting feature with the indirect band gap of 1.07 eV. The underlying metal-to-semiconductor transition in FeB_4 can be evident from the electron localization function (ELF) (Fig. 7, *Right*) that the $I4_1/acd$ phase possesses the considerable localization of electrons near Fe atoms compared with the *Pnnm* counterpart. Under further compression from 53.7 GPa to 300 GPa

PHYSICS

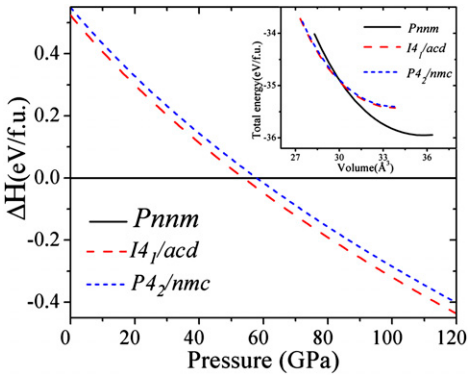

Fig. 4. Relative enthalpies of *Pnnm*, $I4_1/acd$, and $P4_2/nmc$ as a function of pressure referenced to the *Pnnm* phase. (*Inset*) The corresponding energy dependence of volume (E-V).

the gap is observed to be slightly changed by the variation less than 7%, as indicated in Fig. 5*B*. For more reliable band gap and considering the derivative discontinuity of the Kohn–Sham eigenvalue, we are using the screening hybrid functional HSE06 (12). The infinitesimal variation in band gap during the compression can be described by the fact that the $I4_1/acd$ phase is highly incompressible.

The sensitive pressure-induced metal-to-semiconductor transition in FeB_4 may arise from the appreciable variation in bonding features between *Pnnm* and $I4_1/acd$ states. This is clearly seen by the key difference of ELF between *Pnnm* and $I4_1/acd$ shown in Fig. 7, *Right*. In $I4_1/acd$, there is a notable degree of electron localization at the open interstices, but it is minimal near and between ions. This localization is associated with the repulsion between core and valence electrons of neighboring ions at sufficiently high pressure, resulting in enhanced Fe (3*d*)-B(2*p*) hybridization owing to an energy decrement of 3*d* bands with respect to 2*p* bands (1, 13). This effect is apparently evidenced by the significant hybridization between Fe (3*d*)-B(2*p*) close to the Fermi level shown in Fig. 7*C*.

Conclusions

In this work, a systematic density functional theory-driven first principles study leads us to demonstrate an abrupt phase transition of the superhard material FeB_4 under high pressure from conventional superconductor to semiconductor. We have observed strong electron–phonon coupling below 53.7 GPa with orthorhombic *Pnnm* symmetry and a transition to semiconducting phase having $I4_1/acd$ space group symmetry at that particular pressure. The semiconducting phase is dynamically stable up to 300 GPa, which has been confirmed from phonon dispersion calculations. All of the considered structures have been tested to have thermodynamic stability from phonon dispersion calculations. The profound reason behind this exciting phenomenon could be the overlap of atomic cores at higher pressure range, which increases the hybridization of valence electrons and their repulsive interactions with core electrons. The immediate technological outcome of this scenario of metal-to-semiconductor phase transition could be to search for a transparent state of a material that is a metal under ambient conditions. This drastic change of electronic and structural properties can be observed in other materials as well, and hence this could open a field of studying them from a high-pressure perspective.

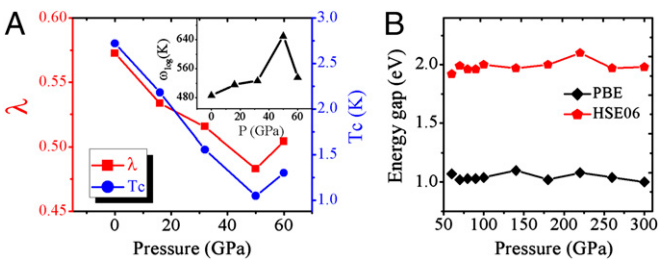

Fig. 5. (*A*) Calculated electron–phonon coupling constants and critical temperatures of the *Pnnm* phase at selected pressures. (*Inset*) The logarithmic phonon momentum (ω_{log}). (*B*) The variation of band gap of the $I4_1/acd$ phase calculated by PBE and HSE06.

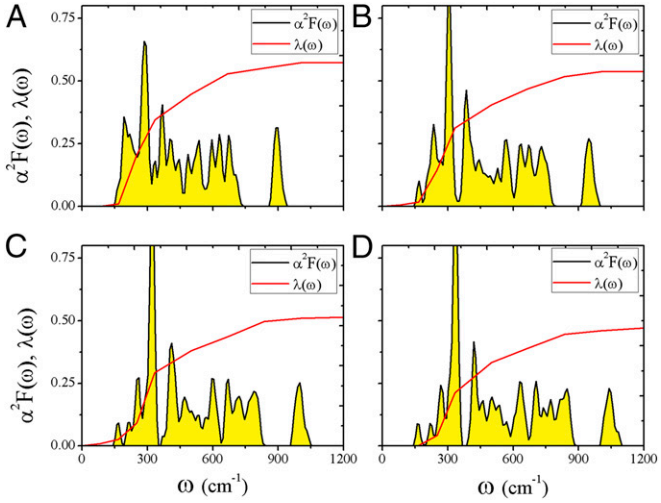

Fig. 6. Calculated spectral function $\alpha^2F(\omega)$ (black line) and integrated $\lambda(\omega)$ of *Pnnm* at selected pressure points (*A*) 0 GPa, (*B*) 16 GPa, (*C*) 32 GPa, and (*D*) 50 GPa.

Materials and Methods

The behavior under high pressure of the *Pnnm* phase has been investigated considering the mechanical property and the electron–phonon coupling

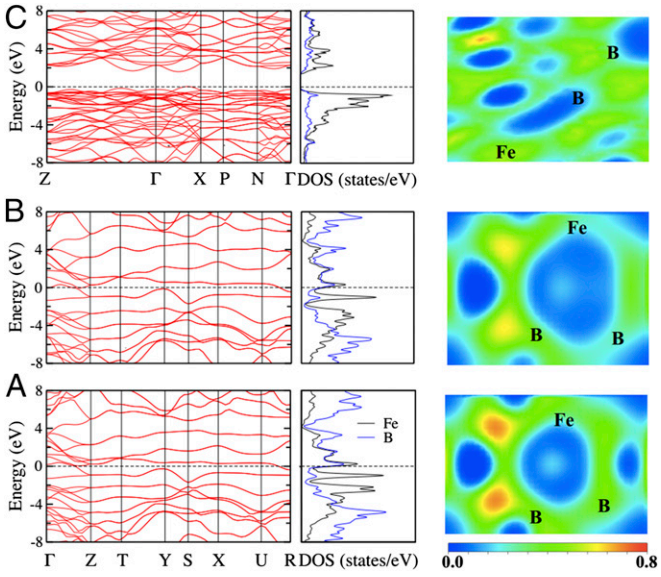

Fig. 7. Electronic band structures, orbitally projected density of states (DOS), and valence electron localization function (ELF) of the *Pnnm* phase at (*A*) 0 GPa and (*B*) 53.7 GPa. (*C*) $I4_1/acd$ phase at 53.7 GPa. The representative lattice planes are (100) and (101) for *Pnnm* and $I4_1/acd$, respectively.

that leads to superconductivity. Moreover, the higher-pressure phase has been predicted using the evolutionary algorithm within the USPEX code (9, 10) with an interface to the projector augmented wave (PAW) method (14) implemented VASP code (15, 16), from 50 GPa to 300 GPa within size cell is up to 8 f.u. (8 of Fe and 32 of B atoms per cell). To obtain reliable and consistent results, the crystal structure of the first two lowest enthalpy phases at each pressure is being accurately optimized. These calculations are performed based on density-functional theory (DFT) formalism. The PAW approach with nonlinear core correction and valence states of Fe ($3p^6 3d^7 4s^1$) and B ($2s^2 2p^1$) have been considered throughout this investigation. The *k*-points mesh and the cutoff energy are $12 \times 8 \times 16$ (for *Pnnm*), $8 \times 8 \times 10$ (for $I4_1/acd$ in primitive cell), $10 \times 10 \times 7$ (for $P4_2/nmc$), and 900 eV, which have been tested to ensure the energy convergence of 1 meV/atom. We have used the Birch–Murnaghan equation of state to fit the energy with respect to the corresponding volume (17). The lowest enthalpy phase is the most stable phase at a specific pressure when considering the profile of enthalpy and pressure for different phases. To confirm the dynamical stability of the most stable phase from the previous structure prediction, we have performed phonon calculations based on the density functional perturbation theory (DPFT) framework as used in Phonopy code (18). To explore the electronic properties of the considered structures, we have performed the band structures and electronic density of states calculations with more accurate *k*-points mesh. We have used PBE (19) type generalized gradient approximation for exchange correlation functional for the electronic structure calculations. For calculating the optical band gap, we have considered the derivative discontinuity of Kohn–Sham energy eigenvalues as formulated in hybrid-type exchange correlation functional HSE06 (20).

Because FeB_4 has been reported as a phonon-mediated superconductor at ambient pressure (4, 5), we have also quantified the electron–phonon couplings of *Pnnm* to elucidate the variation of its superconducting feature with respect to pressure. These calculations are carried out using Quantum Espresso package (21, 22) based on the PAW approach. The cutoff energy is set to be 90 Ryd with the convergence setting of $2 \times 2 \times 4$ *q*-mesh and $6 \times 6 \times 12$ *k*-mesh for the dynamical matrix and $12 \times 12 \times 24$ *k*-mesh for the electron–phonon coupling. The superconducting critical temperature (T_c) has been evaluated by the Allen Dynes formula (23, 24).

ACKNOWLEDGMENTS. The Swedish National Infrastructure for Computing and Uppsala Multidisciplinary Center for Advanced Computational Science are acknowledged for providing computing time. K.K. and T.B. acknowledge assistance from the Thailand Research Fund (TRF) through Royal Golden Jubilee Ph.D. Program Grant PHD/0277/2552 and a 90th Year Chulalongkorn Scholarship. T.B. acknowledges TRF Contract RSA5580014, National Research Council of Thailand, and Ratchadaphiseksomphot Endowment Fund of Chulalongkorn University Grant RES560530180-AM and the Special Task Force for Activating Research, Ratchadaphiseksomphot Endowment Fund, Chulalongkorn University, through the Energy Materials Physics Research Group. T.K., S.C., J.A., P.C.P., W.L., and R.A. acknowledge the Royal Thai Government, Carl Tryggers Stiftelse for Vetenskaplig Forskning, Coordenação de Aperfeiçoamento de Pessoal de Nível Superior, Swedish Research Council, and the Swedish Energy Agency for financial support. This research was supported by the Leading Foreign Research Institute Recruitment Program through the National Research Foundation of Korea funded by Ministry of Education, Science and Technology Grant 2014-039452.

1. Ma Y, et al. (2009) Transparent dense sodium. *Nature* 458(7235):182–185.
2. Neaton JB, Ashcroft NW (1999) Pairing in dense lithium. *Nature* 400:141–144.
3. Ma Y, Oganov AR, Xie Y (2008) High-pressure structures of lithium, potassium, and rubidium predicted by an ab initio evolutionary algorithm. *Phys Rev B* 78: 014102–014105.
4. Kolmogorov AN, et al. (2010) New superconducting and semiconducting Fe-B compounds predicted with an ab initio evolutionary search. *Phys Rev Lett* 105(21):217003.
5. Gou H, et al. (2013) Discovery of a superhard iron tetraboride superconductor. *Phys Rev Lett* 111(15):157002–157005.
6. Zhang X, et al. (2013) First principle study of elastic and thermodynamic properties of FeB_4 under high pressure. *J Appl Phys* 114:183517.
7. Zhang X, et al. (2013) Deformation-induced bonding evolution of iron tetraboride and its electronic origin. *Phys Status Solidi RRL* 7:1022–1025.
8. Ding LP, Kuang XY, Shao P, Huang XF (2014) Structural and relative stabilities, electronic properties, and hardness of iron tetraborides from first prinicples. *Inorg Chem* 53(7):3471–3479.
9. Oganov AR, Glass CW (2006) Crystal structure prediction using ab initio evolutionary techniques: Principles and applications. *J Chem Phys* 124(24):244704.
10. Glass CW, Oganov AR, Hansen N (2006) USPEX evolutionary crystal structure prediction. *Comput Phys Commun* 175:713–720.
11. Watson RE, Fernando GW, Weinert M, Wang YJ, Davenport JW (1991) Local-density approximation: Cohesion in the transition metals and s—>d promotion in the transition-metal atoms. *Phys Rev B Condens Matter* 43(2):1455–1462.
12. Marsman M, Paier J, Stroppa A, Kresse G (2008) Hybrid functionals applied to extended systems. *J Phys Condens Matter* 20(6):064201.
13. Neaton JB, Ashcroft NW (2001) On the constitution of sodium at higher densities. *Phys Rev Lett* 86(13):2830–2833.
14. Blöchl PE (1994) Projector augmented-wave method. *Phys Rev B Condens Matter* 50(24):17953–17979.
15. Kresse G, Furthmüller J (1996) Efficient iterative schemes for ab initio total-energy calculations using a plane-wave basis set. *Phys Rev B Condens Matter* 54(16):11169–11186.
16. Kresse G, Furthmuller J (1996) Efficiency of ab-initio total energy calculations for metals and semiconductors using a plane-wave basis set. *Comput Mater Sci* 6:15–50.
17. Birch F (1947) Finite elastic strain of cubic crystals. *Phys Rev* 71:809–824.
18. Togo A, Oba F, Tanaka I (1996) First-principles calculations of the ferroelastic transition between rutile-type and $CaCl_2$-type SiO_2 at high pressures. *Phys Rev B* 78:134106.
19. Perdew JP, Burke K, Ernzerhof M (1996) Generalized gradient approximation made simple. *Phys Rev Lett* 77(18):3865–3868.
20. Heyd J, Scuseria GE, Ernzehof M (2003) Hybrid functionals based on a screened Coulomb potential. *J Chem Phys* 118:8207.
21. Giannozzi P, et al. (2009) QUANTUM ESPRESSO: A modular and open-source software project for quantum simulations of materials. *J Phys Condens Matter* 21(39): 395502.
22. Methfessel M, Paxton AT (1989) High-precision sampling for Brillouin-zone integration in metals. *Phys Rev B Condens Matter* 40(6):3616–3621.
23. Bullet DW (1977) Relation between electronic structure and T_c in binary and ternary molybdenum chalcogenides. *Phys Rev Lett* 39:664–666.
24. Allen PB, Dynes RC (1975) Transition temperature of strong-coupled superconductors reanalyzed. *Phys Rev B* 12:905–922.